Available online at www.sciencedirect.com
SCIENCE DIRECT
Polymer 46 (2005) 2966–2977
polymer
www.elsevier.com/locate/polymer

Confined crystallization phenomena in immiscible polymer blends with dispersed micro-and nanometer sized PA6 droplets part 4: polymorphous structure and (meta)-stability of PA6 crystals formed in different temperature regions

R.T. Tol, V.B.F. Mathot, H. Reynaers, B. Goderis, G. Groeninckx*

Laboratory of Macromolecular Structural Chemistry, Division of Molecular and Nanomaterials, Department of Chemistry, Catholic University of Leuven, Celestijnenlaan 200F, B-3001 Heverlee, Belgium

Received 24 June 2004; received in revised form 11 January 2005; accepted 1 February 2005
Available online 10 March 2005

Abstract

The genesis and stability of different PA6 crystalline polymorphs, dispersed as micro- and submicrometer sized droplets inside an amorphous polymer matrix, are discussed over a very broad temperature range. Different PA6 droplet sizes lead to different PA6 crystallization events in a 100 °C wide temperature window that extends down to 85 °C. Static WAXD and DSC experiments on micrometer sized PA6 droplets indicate the formation of a stable γ-crystal phase in the region between 175 and 130 °C. Sub-micrometer sized PA6 droplets only crystallize at 85 °C in the β-phase. Upon heating above the PA6 glass transition, these crystals progressively increase their perfection and ultimately transform into the α-phase around 170 °C.

Keywords: PA6 crystal structure; Crystal stability; Melting

1. Introduction

If a semicrystalline polymer is dispersed into confining droplets, strong effects on its crystallization behavior have been observed [1–12]. As a result of the lack of active heterogeneities in the isolated droplets, several crystallization events take place at different lowered temperatures, also referred to as fractionated crystallization [5]. In two recent previous papers [11,12], these phenomena for PA6 droplets dispersed inside different amorphous polymer matrices were investigated. Via reactive compatibilization of the blends, the PA6 droplet size was strongly reduced, resulting in crystallization around 85 °C, more than 100 °C lower than the normal bulk crystallization temperature. In another paper [13], it has been shown that crystallization at these low temperatures exhibits sporadic nucleation kinetics, characteristic for homogeneous nucleation. As a result of the low crystallization temperatures and the small size of the PA6 droplets, imperfect crystals are formed, resulting in a low final crystallinity.

For polymorphous semicrystalline polymers, like PA6, the different crystalline structures formed during the cooling step and their stability, which in general strongly depend on crystallization conditions like temperature and cooling rate, are of great importance for the final properties. Browsing the literature on the crystal structures of PA6 confirms the complexity of the issue at hand. Contradictory results are found as well. The monoclinic α- structure is well characterized and is obtained as the major crystal fraction in moderately or slowly cooled PA6 samples. It is a stable structure with a relatively high density of approximately 1.23 g/cm^3 [14,15]. The melting enthalpy of 100% crystalline α-phase, $\Delta h(T_m^\circ)$ is found to be 230 J/g [16] with an experimental melting point, T_m, of 223 °C. The reported T_m° is 260–270 °C [16]. The stable monoclinic γ-phase is also well characterized and is obtained by a KI/I_2 water solution treatment of α-crystals [17–20]. The melting temperature of this form is determined to be approximately 214 °C, with a

* Corresponding author. Tel.: +32 16 327440; fax: +32 16 327990.
E-mail address: gabriel.groeninckx@chem.kuleuven.ac.be (G. Groeninckx).

0032-3861/$ - see front matter © 2005 Elsevier Ltd. All rights reserved.
doi:10.1016/j.polymer.2005.02.021

density of about 1.19 g/cm^3 [19,21,22]. The corresponding $\Delta H(T_m^\circ)$ equals 239 J/g according to calculations by Illers et al. [14]. This value, however, is affected by the density assumed. In addition, several authors have proposed a third form, β, mostly obtained after fast quenching or cold crystallization of PA6 [15,23–25]. The precise characterization of this structure is heavily disputed, because the WAXD profile is comparable to that of the γ-form. Mostly, a mesomorphic, (pseudo)hexagonal structure is proposed [25], which is very unstable compared to the stable γ-form obtained via the aqueous KI/I_2 treatment of α-crystals, and which will give the α-structure upon annealing. Various authors, however, have come up with different structures such as paracrystalline monoclinic α [24], pseudohexogonal γ* [14,19], pleated α [26], leading to a confusing nomenclature.

Another group of authors states that the various structures found are nothing more than α or γ-structures with various degrees of perfection and can be viewed as intermediate structures between the two stable forms with respect to the H-bond setting and chain conformation [27–29]. Murthy et al. [27] propose a disordered metastable phase and show that the stable γ form can be reversibly transformed into this form by applying shear.

Penel-Pierron et al. [30] summarize that although the γ-form is crystallographically similar to the unstable mesomorphic β-form, the β-form chain conformation must strongly resemble amorphous material as Infrared spectroscopy is hardly able to discriminate such material from the amorphous phase [31]. FTIR, however, is able to separate γ and β-structures [32]. Illers et al. [14] propose a value of 60 J/g for the $\Delta H_{100\%}$ of the unstable form, labelled γ*, based on the specific volume.

The above summary of literature shows the high complexity of the polymorphous structures of PA6. In almost all cases mixtures of α-like and γ-like phases of different order are found, strongly depending on the crystallization conditions, such as the crystallization temperature, cooling rate [14,19,21,33–37], shear rate [22,26,29,31,38–40], humidity [22,35,41] and pressure [40].

It will be shown and emphasized in this paper that the occurrence of crystallization in different separated temperature intervals for isolated, dispersed PA6 droplets in amorphous polymer matrices can be an alternative and very effective approach to study the formation and stability of the different polymorphous crystalline structures of PA6. The blend systems considered cover a broad range of both PA6 droplet sizes (between 0.1 and 10 μm) as well as PA6 crystallization temperatures (between 80 and 185 °C). First, the determination of the crystal structures of PA6 droplets during crystallization in different temperature intervals will be presented. Decomposition of static WAXD profiles will provide the fractions of the different crystalline phases as well as the crystallinities of PA6 in the blends. In the second part of this paper, the stability of the crystal structures formed at different temperatures is investigated using DSC at different cooling and heating rates combined with static WAXD experiments.

2. Materials and methods

2.1. Materials, blend preparation and characterization

Polyamide-6 (PA Akulon K123) was provided by DSM Research. Atactic polystyrene (PS Styron E680) was supplied by DOW Benelux and poly(2,6-dimethyl-1,4-phenylene ether) (PPE) by General Electric Plastics. The miscible polystyrene/polyphenylene-ether (PPE/PS) 50/50 wt/wt mixture was prepared by mixing PPE and PS in a Haake Rheocord 90 twin-screw extruder [42]. Styrene-maleic anhydride copolymer SMA2 was provided by Bayer. The number after SMA denotes the wt% maleic anhydride in SMA. Talc powder was kindly provided by DSM Research. Using optical microscopy, the size of the talc particles was estimated to vary between 0.1 and 1 μm.

Uncompatibilized PS/PA6 and (PPE/PS)/PA6 blends as well as reactively compatibilized samples with SMA2 have been investigated. The two-phase blends were prepared on a co-rotating twin-screw mini-extruder manufactured by DSM Research. A complete description of the material characteristics and processing conditions can be found in a previous paper [43]. In most of these blend systems, PA6 formed droplets inside the amorphous matrix. Averages and distributions of PA6 droplet sizes were obtained by image analysis of SEM pictures, of which a detailed description is also presented in [43].

2.2. Thermal analysis

DSC measurements were performed with a Perkin Elmer Pyris 1. The nitrogen flow-rate was 20 mL/min. Temperature and enthalpy calibration was performed with indium (T_m = 156.6 °C) and tin (T_m = 231.88 °C) at a heating rate of 10 °C/min. Furnace calibration was performed between 0 and 290 °C. The samples were first heated at a rate of 40 °C/min to a melt temperature of 260 °C, and kept there for 3 min in order to erase the sample history. Subsequently, different thermal procedures were applied. (1) Cooling (at different rates) (0.1 and 10 °C/min) to below $T_{g,PA6}$ followed by heating with different rates (10, 20, 40, 100 °C/min) (Section 3.2.1 and 3.2.2). (2) Cooling to different temperatures between $T_{c,bulk}$ and $T_{c,hom.}$ at 10 °C/min, followed by immediate heating at 10 °C/min, to link crystallization and melting of the different crystallizing droplet fractions (Section 3.2.3). (3) Cooling with 10 °C/min to different temperatures between $T_{c,bulk}$ and $T_{c,peak\ 2}$ followed by isothermal crystallization and subsequent heating at 10 °C/min (Section 3.2.1).

Sample masses of about 5 mg were used for a cooling/heating rate of 10 °C/min. Weighing was done with an AND Hm-202 Balance at an accuracy of 0.01 mg. The

sample mass was increased or decreased according to the applied cooling or heating rate (~5 mg for 10 °C/min, ~0.5 mg for 100 °C/min and ~15 mg for 0.1 °C/min). For the various cooling or heating rates used, calibration in heating at the respective rate was applied. DSC curves were corrected for instrumental curvature by subtracting empty-pan curves, measured using identical thermal histories at the beginning and end of each day. A normal calibration set-up at 10 °C/min heating rate was used for calibration of isothermal crystallization but the isothermal temperature was each time set corresponding to the real sample temperature (sensor) instead of the DSC program temperature.

The mass fraction crystallinity of PA6 in the blends after isothermal crystallization was calculated using the temperature dependent Δh values for fully amorphous and fully crystalline PA6 available from the ATHAS databank [44] according to:

$$\omega_c(T) = \frac{\Delta h_{exp}(T)}{\Delta h(T)} \quad (1)$$

with $\Delta h(T) = h_a(T) - h_c(T)$, the difference between the enthalpy at T of fully amorphous and fully crystalline PA6, respectively.

In case of calculating the crystallinity from the melting peak, T was taken equal to $T_{m\ (peak\ max)}$ and recrystallization exotherms were subtracted for calculating Δh_mexp.

For this calculation, the denominator of Eq. (1), $\Delta h(T)$, for the monoclinic γ-phase of PA6 was taken equal to that of the monoclinic α-phase of PA6. This is justified by literature data: $\Delta h(T_m^\circ)_{\alpha\text{-phase}} = 230$ J/g [16] and $\Delta h(T_m^\circ)_{\gamma\text{-phase}} = 239$ J/g [14].

2.3. Static WAXD experiments

Static WAXD measurements at room temperature were performed on a Rigaku Rotaflex Cu-200B rotating anode operated at 40 kV and 100 mA. The incident X-rays (λ = 0.15418 nm) from the Cu-target were monochromatized using a Ni filter. Samples of 1 mm thickness were prepared by compression moulding at 260 °C (4 min) and subsequently given a thermal treatment in a Mettler FP-90 hot stage under N_2-flow similar to the thermal history as in DSC. WAXD patterns were recorded in transmission mode using a Bragg–Brentano focusing diffractometer with a scintillation counter at a step scan size of 0.05° between 3 and 40° 2θ, and a measuring period of 30 s. The PA6 pattern was extracted from the blend diffraction patterns as follows. First an empty sample holder measurement (background) was subtracted from all blend measurements and from the separately measured non-crystallizable components (PS or PPE/PS) after multiplying the background with the sample transmission. Next an additional, linear background was subtracted, connecting the intensities at 2θ = 5° and 2θ = 35°. Finally, the contribution of the non-crystallizable component (PS or PPE/PS) was subtracted after scaling the corrected patterns at 7.5 ° 2θ since PA6 does not scatter significantly at this angle.

The PA6 (X_{cWAXD}) crystallinity was estimated from the ratio of the area under the crystalline peaks to the total area under the PS or PPE/PS stripped WAXD curve. The crystalline peaks and the amorphous halo were fitted with the Origin 6.0 Peak-fitting software package (Microcal Software Inc. USA). The shape of the PA6 amorphous halo was obtained from a very thin quenched PA6 film as shown in Fig. 1 and approximated by a combination of three separate Pearson 7 peaks, of which the shapes and relative peak areas were fixed in the fitting procedure of the blends. The crystalline reflections were fitted with Gaussians. Examples of fitting results are presented in Fig. 2 for PA6 (A) and a PS/PA6 blend (B), respectively. The fractions of different polymorphic phases (α,γ) in PA6 as indicated in Fig. 2 (see Ref. [45] for overview of γ and α-positions), were determined by dividing the area under the α or γ typical reflections by the total crystalline area. The PA6 WAXD contributions were normalized to their total area for representation further in this work.

2.4. Annealing experiments below $T_{m,peak}$ bulk PA6

Annealing experiments below the bulk T_m of PA6 were performed both for DSC as WAXD samples. For the WAXD samples, the compression moulded sample, after being subjected to the standard DSC thermal treatment, was heated to the annealing temperature at a rate of 10 °C/min in the Mettler FP-90 hot stage under N_2-flow, and kept at this temperature during a selected period of time (mostly 4 h). Afterwards, the sample was cooled down to room temperature at 10 °C/min and analyzed by WAXD. For the DSC annealing experiments, the same procedure was applied, by using the DSC throughout, after the standard thermal treatment. The latter results were compared to samples that were quickly quenched below $T_{g,PA6}$ and heated in the DSC with 10 °C/min subsequently.

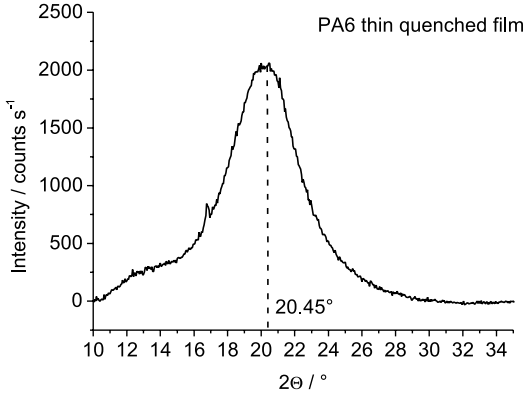

Fig. 1. WAXD profile at RT of quenched PA6.

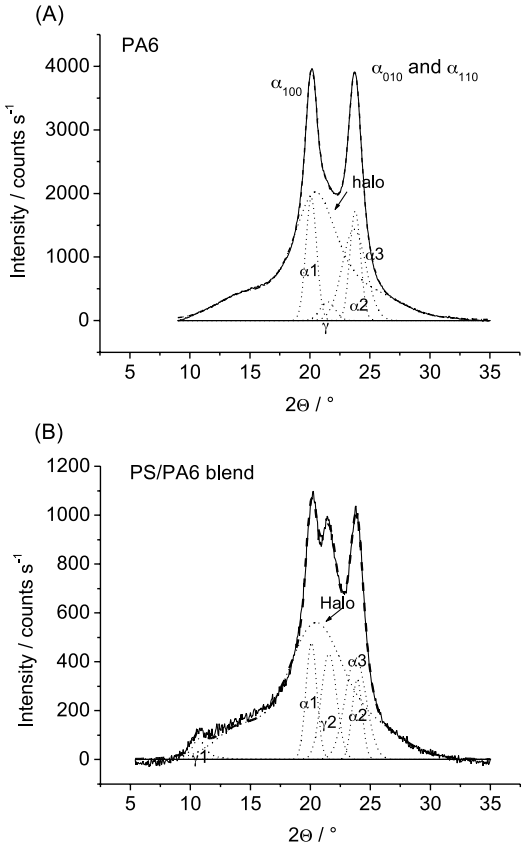

Fig. 2. PA6 WAXD profiles at RT of PA6 (A) and of a PS/PA6 blend (B).

3. Results and discussion

3.1. Polymorphous structure and crystallinity of PA6 as a function of the blend composition using static WAXD experiments

Fig. 3(A) shows the normalized WAXD profiles of PA6 for different PS/PA6 blend compositions determined at room temperature after cooling from 260 °C at 10 °C/min. Besides bulk crystallization of PA6 around 188 °C, a second crystallization peak is found around 170 °C when PA6 forms droplets inside the PS matrix. This is shown in Fig. 3(B) showing the corresponding DSC cooling curves. The 170 °C peak grows in intensity the smaller the PA6 droplet size becomes. The reason for the fractionated crystallization behavior can be related to the lack of active heterogeneous nuclei in most of the dispersed PA6 droplets, as discussed in detail in Refs. [11,12].

The WAXD spectrum of extruded PA6 shows reflections at 20.0 and 23.9° 2θ, characteristic of the monoclinic α-phase of PA6 [45]. A small reflection around 21.4° 2θ is observed, typical for the PA6 γ-phase [45]. When PA6 forms droplets, the reflections of this phase, found at 21.4° and also at 11° 2θ [45], grow in intensity and at the expense of the intensities belonging to the α-phase with decreasing PA6 concentration. At first sight, the formation of the γ-phase reflections found here, seems to be connected to the formation of PA6 droplets and concomitant confinement brought about. More likely, however, is that the formation of the γ-phase is induced by crystallization at a lower temperature, namely around 170 °C for PS/PA6 blends, as caused by the fractionated crystallization. A clear proof of this is obtained when the nucleation density of the blends with PA6 droplets—of unaltered size—is increased, causing suppression of the fractionated crystallization phenomena (see [11]). As a result of such increased nucleation density, complete bulk crystallization of PA6 around 188 °C is reintroduced in the droplets. For example, the WAXD spectrum of the PS/PA6 75/25 blend nucleated with 0.5 wt% talc powder (Fig. 4) shows the presence of the monoclinic α-phase and an almost complete disappearance of the γ-phase reflections (see also Table 1).

An interesting result is given in Fig. 5 where the DSC crystallization curves and the related WAXD spectra are compared for virgin and extruded PA6. It was found that the crystallization behavior of PA6 changed significantly upon melt-extrusion in the twin-screw extruder. After extrusion, PA6 exhibits a higher crystallization temperature; about 15 °C compared to the virgin PA6. This effect has also been found by other authors, and has been explained by a more ordered molecular arrangement that persists in the molten state due to the stabilizing effect of hydrogen bonding after melt-extrusion of PA6 [46,47]. The virgin material is

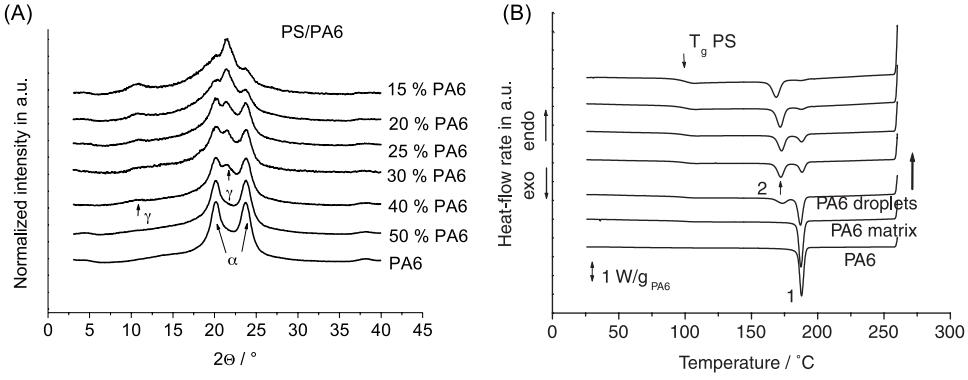

Fig. 3. PA6 WAXD profiles at RT (A) and DSC cooling curves (B) of various PS/PA6 blend compositions and blend morphologies as indicated.

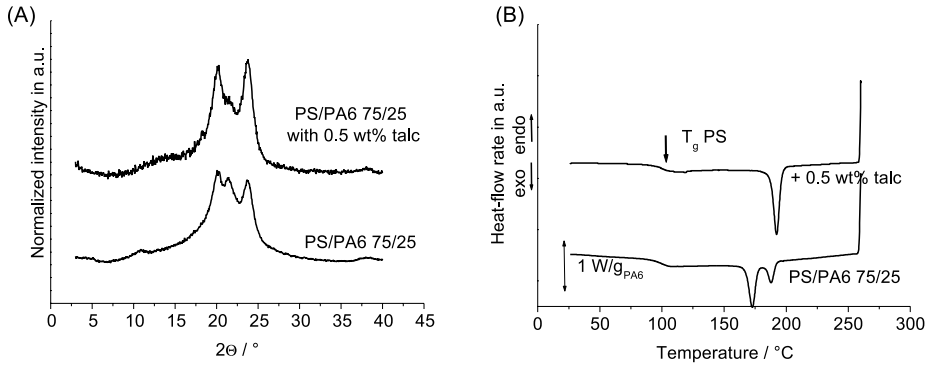

Fig. 4. PA6 WAXD profiles at RT (A) and DSC cooling curves (B) of a PS/PA6 75/25 blend, with and without talc addition.

thought to be disordered and to stay disordered in the molten state, again due to hydrogen bonding. Melt-extrusion is supposed to yield locally ordered regions, which are presumed to act as nucleating sites, causing an increase in the crystallization rate, and also leading to smaller spherulitic structures. Interesting enough Fig. 5 shows that almost no γ-reflections are observed for the virgin PA6 at 170 °C, contrary to extruded PA6 in the blends that crystallizes at the same temperature. So the extrusion processing changed the temperature range in which the different polymorphous structures were obtained.

Fig. 6 shows the normalized WAXD profiles of the PS/PA6 blend series after reactive compatibilization with approximately 5 wt% SMA2, together with the corresponding crystallization curves (cooling rate 10 °C/min). As shown in [43], compatibilization with SMA2 strongly reduces the dispersed droplet size of PA6. The crystallization behavior is characterized by a clear transition from bulk to fractionated crystallization when PA6 forms very small droplets (~150 nm). Crystallization in these very small PA6 droplets mainly takes place via a homogeneous nucleation mechanism, at very low temperatures (in between 85 and 100 °C) [13]. The more SMA2 is added, the smaller the droplet size, and the stronger the homogeneous nucleation peak. The WAXD profiles indicate a clear transition from the α-phase, obtained when PA6 forms the matrix or is co-continuous (and thus crystallizes at the bulk temperature), to an almost complete γ-phase in small droplets, crystallizing at a high degree of supercooling. The fraction of γ-phase thus strongly increases at lower crystallization temperatures at the expense of the α-phase. This confirms the observations made by several authors [21, 33–35], indicating the formation of the γ-form at low crystallization temperatures reached by rapidly cooling from the melt.

The mass percentage crystallinities and relative fractions of the α and γ-phases obtained with WAXD for the uncompatibilized and reactively compatibilized PS/PA6 blend series are given in Table 1. It is seen that the crystallinities obtained from the DSC melting data correspond reasonably well with the values obtained from WAXD, with exception of the data of the very small droplets, in case of compatibilized blends. Here the WAXD crystallinity is significantly lower than the DSC

Table 1
WAXD results for PS/PA6 and (PS/SMA2)/PA6 blend compositions

Blend system	Wt% PA6	D_v PA6 (μm)	Cooling rate 10 °C/min			
			% α	% γ	$X_{c,WAXD}$	$X_{c,DSC}$[a]
PA6	100	–	93	7	36	35
PS/PA6	50	Matrix	80	20	35	33
	40	25	70	30	33	30
	30	7.6	69	31	24	27
PA6 dispersed	25	5.0	63	37	27	24
	25+ talc	5.2	82	18	34	32
	20	3.3	42	58	22	23
	15	3.0	22	78	22	23
(PS/SMA2)/PA6	45[b]	Co-cont.	89	11	33	33
	40[b]	0.55	37	63	25	25
PA6 dispersed	30[b]	0.21	29	71	23	25
	25[b]	0.18	24	76	17	27
	25[c]	0.16	16	84	16	25

[a] Determined from melting peak.
[b] ~5 wt% SMA2.
[c] 13 wt% SMA2.

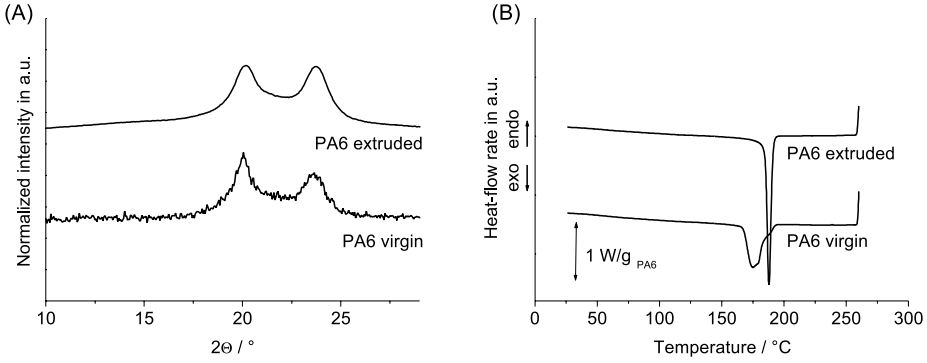

Fig. 5. WAXD profiles at RT (A) and DSC cooling curves (B) of PA6 extruded and PA6 virgin.

crystallinity. This interesting observation will be discussed further in Section 3.2.

3.2. Melting and (meta)stability of PA6 crystals in different temperature domains

3.2.1. PA6 and uncompatibilized PS/PA6 and (PPE/PS)/PA6 blends: high and intermediate crystallization temperatures

Fig. 7 shows the DSC melting curves of PA6 and the PS/PA6 blend series as a function of the blend composition. The corresponding crystallization curves are presented in Fig. 3. For pure, extruded PA6 a double melting with maxima at T_{m1} and T_{m2} is observed, which is always accompanied by a small endotherm around 180–190 °C, prior to full melting. Fig. 8 shows the melting of extruded PA6 after applying different heating rates. For PA6 a relative increase of the first melting peak area is found upon faster heating at the expense of the second one, and, the other way around, an increase of the second melting peak area at low heating rates. The melting behavior of PA6 after crystallization at a low cooling rate of 0.1 °C/min mainly displays the melting peak at the highest temperature (T_{m2} = 222 °C), though the little shoulder resembling T_{m1}, is still seen.

These results clearly indicate recrystallization of PA6 crystals as the main origin of the double melting behavior; less perfect α-crystals, formed in the cooling step, will melt (at maximum rate at T_{m1}) and form more stable crystals by recrystallization that finally melt around T_{m2}. Slow cooling (at 0.1 °C/min) will most likely result in the formation of crystals of higher perfection. As a result, there is hardly any recrystallization and a major melting peak is found at the highest temperature, as shown.

Some remarkable changes in PA6 melting behavior are found when PA6 forms droplets. A progressive increase of the first melting peak at approximately 210 °C can be observed with decreasing PA6 contents. This effect is accompanied by an exotherm prior to the onset of melting. For pure PA6 this exotherm was not observed during the heating scan. When comparing the blend morphology of the PS/PA6 blend compositions with the obtained melting plots, it is notable that a strong increase in intensity of the first melting peak is related to the formation of dispersed PA6 droplets, mostly crystallizing around 160–170 °C. In Fig. 9 it can be seen that the evolution of the lower temperature melting peak can be connected to the crystallization event around 170 °C. In this figure the shape of the melting peak is recorded after different isothermal crystallization temperatures. Fig. 9(A) shows the data for pure PA6. For isothermal temperatures T_{iso} = 205, 200 and 195 °C (the latter is the onset of bulk crystallization upon a cooling scan of 10 °C/min, which is indicated with the horizontal dashed line) one melting peak is found and a low temperature shoulder. Peak

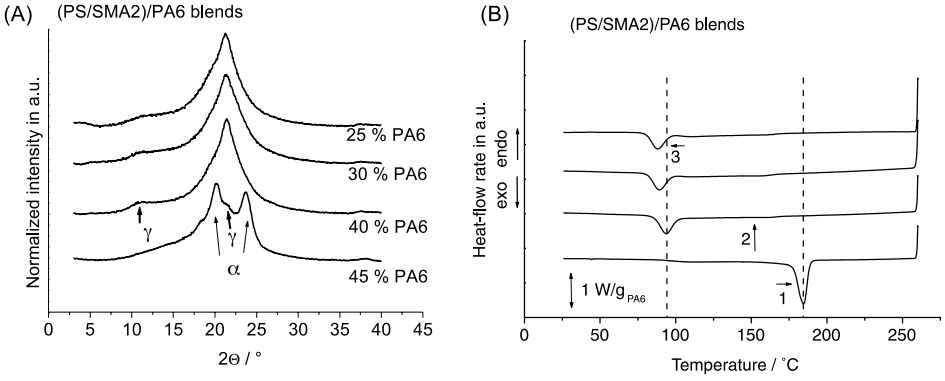

Fig. 6. PA6 WAXD profiles at RT (A) and DSC cooling curves (B) of different (PS/SMA2)/PA6 blend compositions.

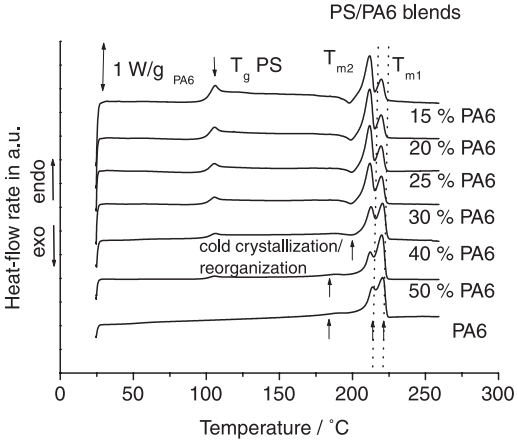

Fig. 7. DSC melting curves of different PS/PA6 blend compositions.

1 is the final melting peak of the crystals formed in isothermal crystallization. The shoulder (peak 3) is the typical 'annealing' peak found after isothermal crystallization, typically about 10 °C above the crystallization temperature. A second melting peak (peak 2) is observed for $T_{iso} \leq 195$ °C. By lowering to this isothermal temperature, part of the crystals has been crystallized during cooling. As such, peak 2 relates to the melting of crystals crystallized on cooling. The crystals formed during the cooling run can recrystallize, and finally melt at peak 1*. By lowering T_{iso} to 175 °C, all material is crystallized during cooling, further enhancing the recrystallization melting peak 1*.

For the PS/PA6 85/15 blend, shown in Fig. 9(B), the melting behavior is similar to the PA6 behavior down to a temperature T_{iso} of ~185 °C. The evolution of the melting enthalpy down to T_{iso} ~185 °C corresponds to the crystallization of the bulk peak, which area is strongly decreased, because almost all material crystallizes at a lower temperature via fractionated crystallization. The second lower crystallization peak shows an onset at ~175 °C upon cooling at 10 °C/min. These onsets are indicated in Fig. 9 with horizontal dashed lines. For $T_{iso} = 175$ °C, a change in melting behavior can be observed. Peak 2 starts to increase

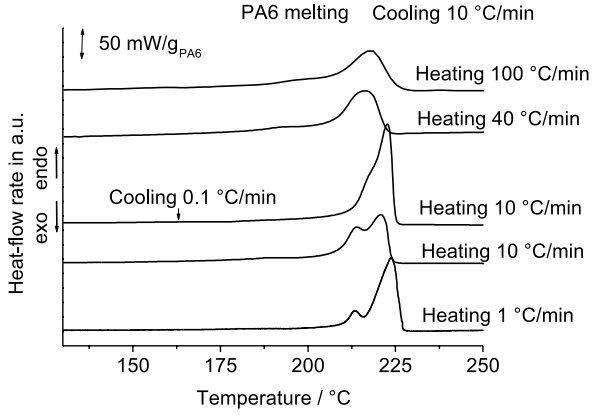

Fig. 8. DSC melting curves of PA6 after different cooling and heating rates.

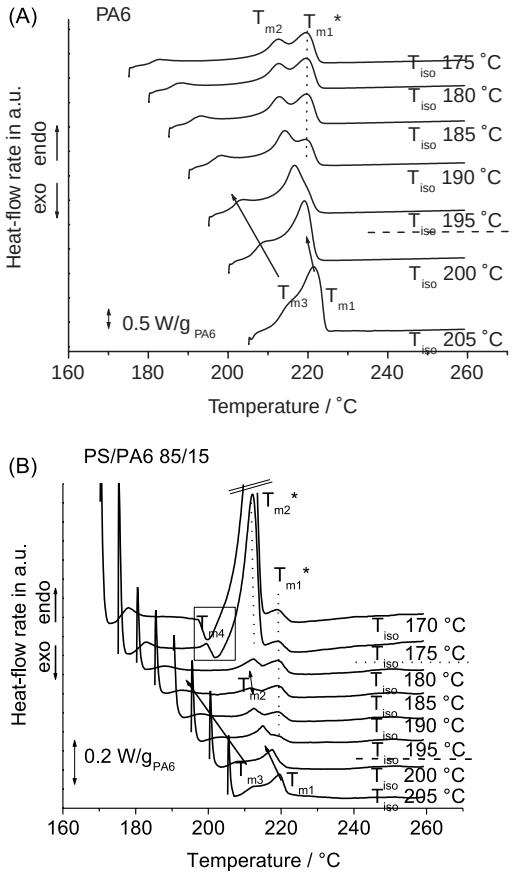

Fig. 9. DSC melting curves at 10 °C/min after isothermal crystallization for 120 min at the indicated temperatures for PA6 (A) and of a PS/PA6 85/15 blend (B) – – – (dashed line): onset bulk crystallization, 10 °C/min cooling rate, … (dotted line): onset crystallization peak $_2$, 10 °C/min cooling rate.

and an extra melting peak is observed (peak 4), accompanied by a cold crystallization exotherm. The position of this extra melting peak decreases with decreasing crystallization temperature. The strong increase of peak 2 must be related to the isothermal crystallization of the lower temperature (fractionated) peak. Lowering T_{iso} further to 170 °C, causes a large part of the second peak to be realized during cooling and yields about the same melting enthalpy, compared to $T_{iso} = 175$ °C.

Together with the results obtained with WAXD (Fig. 3), these observations lead to the conclusion that the first melting peak is related to the melting of the monoclinic γ-phase around 210 °C, comparable to the monoclinic γ-phase via iodinization of α crystals, characterized by Illers et al. [19] (reported melting T_m (γ) = 214 °C). The exotherm prior to melting can probably be related to reorganization of less perfect γ-crystals, which subsequently melt around 210 °C. This last hypothesis is confirmed by the observation that the larger the pre-melting exotherm, the larger the first melting peak becomes. This explanation (relating the origin of the exotherm to reorganization) is similar to the one recently proposed by Penel-Pierron et al. [30] for cast PA6 films. These authors doubted the explanation of Khanna et al. [48],

relating the presence of the exotherm to the relaxation of internal stresses, locked during processing.

By applying various heating and cooling rates in the DSC, clear evidence can be obtained that the melting peak at 210 °C is mainly related to the melting of γ-crystals formed at 160–170 °C, and less to melting-recrystallization of imperfect α-crystals. Fig. 10 shows the effect of different heating rates and cooling rates on the melting behavior of the PS/PA6 75/25 blend. This blend contains both α and γ-crystallites as can be seen in Fig. 3 and Table 1. Qualitatively, the effect of the heating rate does not differ that much from the pure PA6 data (Fig. 8); again the lower melting peak rises in intensity upon increasing the heating rate whereas the second one decreases. This effect is due to the recrystallization of the α-phase only. Closer inspection of the melting trace recorded at 100 °C/min—when recrystallization is avoided—reveals that it is very skew towards low temperatures (210 °C), suggesting an important fraction of crystals with a melting behavior that is not influenced by the heating rate (the γ-phase crystals). Moreover, the ratio of the two melting peaks does not change so much upon slow cooling for the PS/PA6 75/25 blend, contrary to the PA6 behavior. The main effect is that the exotherm prior to melting disappears. As such, the first melting peak cannot solely be attributed to the melting of less perfect α crystals formed during cooling that recrystallize and remelt in the second peak, which was the case for pure PA6. The amount of γ-phase formed upon cooling at 0.1 °C/min is not expected to be very different from the fraction γ-phase obtained after cooling with 10 °C/min in this PS/PA6 75/25 blend, because the position (and also intensity) of the second crystallization peak around 170 °C is very insensitive to the applied cooling rate (between 0.1 and 10 °C/min), as was shown in [11]. This result thus furthermore confirms the hypothesis made earlier, linking the melting peak at 210 °C to the melting of the stable γ-phase, which does not convert to α-crystals upon heating (the stability of the crystals upon heating will be further investigated in Section 3.2.3 using WAXD annealing experiments). The low cooling rate increases the perfection of the γ-crystals formed upon crystallization compared to cooling at 10 °C/min, which explains the absence of the reorganization exotherm in this curve. Upon fast heating (after cooling at 10 °C/min), which likely prevents the reorganization of the less perfect γ-crystals, the exotherm prior to melting also disappears. The endotherm in this fast heating scan (see arrow in Fig. 10) can probably be related to the melting of the less perfect crystals formed during cooling at 10 °C/min. Similar extra melting peaks for PA6 were also reported by Weigel et al. [21] for crystallization at lower temperatures, after quick cooling from the melt state to T_{iso}. Up to five melting peaks were reported for melt-crystallized samples at different temperatures and were related to the melting phenomena of different γ or α-crystals (see Ref. [16], page 70–71 for a summary).

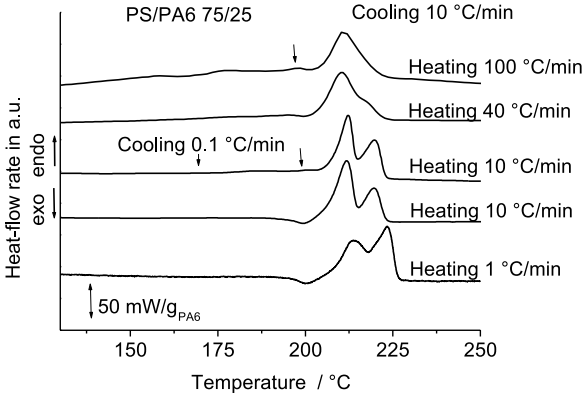

Fig. 10. DSC melting curves of a PS/PA6 75/25 blend after different cooling and heating rates.

3.2.2. Reactively compatibilized (PS/SMA2)/PA6 blends: low crystallization temperatures

Fig. 11(A) shows the effect of compatibilization on the melting behavior of the (PS/SMA2)/PA6 75/25 blends, in which PA6 is dispersed as droplets. The crystallization curves are plotted below the melting curves for comparison in Fig. 11(B). Addition of only a small amount of compatibilizer SMA2 already significantly reduces the

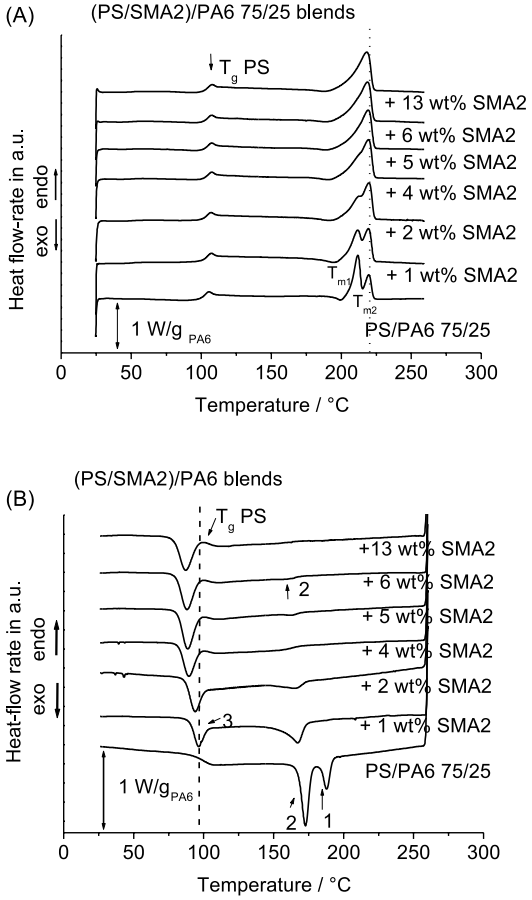

Fig. 11. DSC melting (A) and cooling (B) curves of different (PS/SMA2)/PA6 75/25 blends with various SMA2 concentration.

droplet size, leading to a stronger fractionated crystallization effect. This causes an increase in the relative amount of the low temperature crystallization peak at 85 °C with increasing SMA2 concentration, at the expense of the peaks at 188 °C (bulk) and 170 °C [12]. The melting behavior shows an interesting evolution as a function of the amount of compatibilizer added. With increasing amount of compatibilizer, the relative intensity of the first melting peak at 210 °C (related to the monoclinic γ-phase as discussed in the previous part) decreases, until finally a single melting peak is obtained at the highest temperature (~220 °C). It is quite remarkable that although the PA6 droplets crystallize at a very low temperature, the melting of the droplets is found to take place around the normal melting peak, with a difference $\Delta T=(T_m-T_c)=(220–85\ °C)=135\ °C$. The melting of these crystals, which showed typical γ WAXD reflections as shown in Fig. 6, apparently does not give rise to a melting peak of stable γ- crystals around 210–215 °C, as for the uncompatibilized droplets. Interestingly also, the crystallization exotherm prior to the onset of melting, which was connected to the cold crystallization of less perfect γ-crystals previously, decreases in intensity upon addition of more compatibilizer.

3.2.3. Determination of stability of the polymorphous phases with DSC

The absence of the typical γ-peak around 210 °C upon melting of PA6 crystallized at low temperatures, points to a lower stability of the γ-like crystals upon heating. As such, the structure formed at the homogeneous nucleation temperature could be similar to the proposed β-form found during cold crystallization of PA6, which was transformed to the α-phase upon heating. The following DSC experiment has been performed to investigate in which temperature range the transition from relatively stable γ-crystals to the unstable β/γ-like crystals takes place. Fig. 12 shows the melting behavior of the (PPE/PS)/PA6 80/20 blend, cooled to different temperatures. In [11] it was found

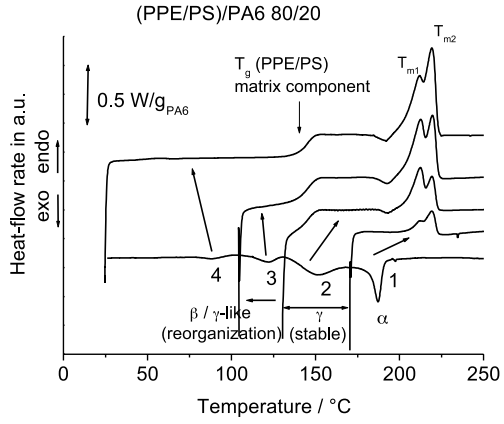

Fig. 12. DSC melting curves of a (PPE/PS)/PA6 80/20 blend after cooling to various temperatures. Bottom curve reflects various fractionated crystallization events during cooling (1→4).

that this blend composition exhibits up to four crystallization peaks: at 187 °C (peak no.1), 160 °C (peak no.2), 122 °C (peak no.3) and 89 °C (peak no.4), respectively, see bottom curve in Fig. 12. Upon cooling to about 170 °C, only bulk crystallization has taken place for this blend, and a small double-peaked endotherm is measured via the subsequent heating run, with an area comparable to the bulk crystallization exotherm. Cooling down to 130 °C causes an overall increase in the melting endotherm, while it is seen that especially the first melting peak (T_{m1}) increases. This is explained by the crystallization into the γ-form at temperatures between 170 and 130 °C, as a result of fractionated crystallization, causing a melting endotherm at 210 °C. Below 130 °C, the crystallization enthalpy starts to become considerably smaller than the subsequent enthalpy from the melting peak area resulting from that crystallization. This can be calculated from the areas under the crystallization and melting peak, respectively. The exotherm prior to melting also increases in intensity. Cooling down to 100 °C causes a further increase in the melting endotherm due to crystallization of peak 3, but now especially the second melting peak (T_{m2}) increases compared to the first one. Crystallization down to room temperature followed by heating even more increases melting peak T_{m2}. The disordered structure formed at these high supercoolings is obviously very prone to reorganization during heating, causing the second melting peak to increase in intensity. The transition between crystallization into γ-crystals, melting around 210 °C, and crystallization into γ-like/β-crystals resulting in a melting peak around 220 °C with twice the intensity of the crystallization peak, thus seems to take place around a crystallization temperature of 130 °C. Interestingly, this temperature coincides with the reported maximum temperature for homogeneous nucleation in PA6 [2].

3.3. WAXD and DSC annealing experiments

To further investigate the stability of the polymorphous structures of PA6 formed at different crystallization temperatures, WAXD and DSC annealing experiments were performed. Fig. 13 shows the WAXD profiles for the compatibilized (PS/SMA2)/PA6 75/25 blend that crystallizes at 85 °C and that was given annealing treatments at different temperatures below the melting point. Prior to annealing, the samples were first cooled down to room temperature at 10 °C/min (standard temperature procedure). Above an annealing temperature of 170 °C, the γ-like reflections at 11 and 21.4° 2θ completely disappear as a function of time, resulting in fully α-reflections at 19.8 and 23.9° 2θ. This transformation is quite fast, and already after an annealing time of 60 s an appreciable transformation has taken place into the α-form (18% γ-type crystals left after 60 s). These results clearly further confirm the formation of a less stable structure with an identical WAXD pattern as the γ-form at lower crystallization temperatures, which is

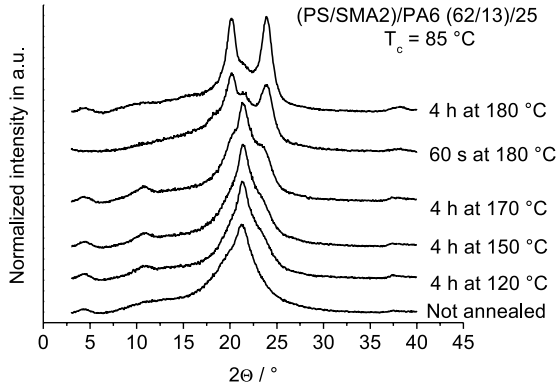

Fig. 13. WAXD crystallinity at RT after annealing as a function of annealing temperature for PA6, a PS/PA6 75/25 blend and a (PS/SMA2)/PA6 (62/13)/25 blend.

transformed into the α-phase upon heating. Annealing also results in a remarked increase in crystallinity, from approximately 10% after cooling to room temperature, up to 35–40% after annealing below T_m. This points to a significant amount of reorganization of crystals and cold crystallization during the heating process, which starts already above 100 °C, as can be seen in Fig. 14. Continuous reorganization obscures the real melting of the low temperature crystals and leads to a final melting temperature far above the crystallization temperature, as was shown in Fig.11. Further evidence for these reorganization phenomena in this blend system was already presented in [13]. Reorganization in heating also explains the remarked difference between crystallinity values obtained with WAXD after cooling and with DSC after melting as indicated in Table 1 for blends with small, dispersed PA6 droplets.

Fig. 15 shows the annealing behavior of the PS/PA6 75/25 blend with droplets of ~1–5 μm and crystallizing between 185 and 170 °C (two peaks), and of the (PS/SMA2)/PA6 75/25 blend with only 1 wt% SMA2 (74/1/25), with droplets of ~0.5 μm [12], and crystallizing partly

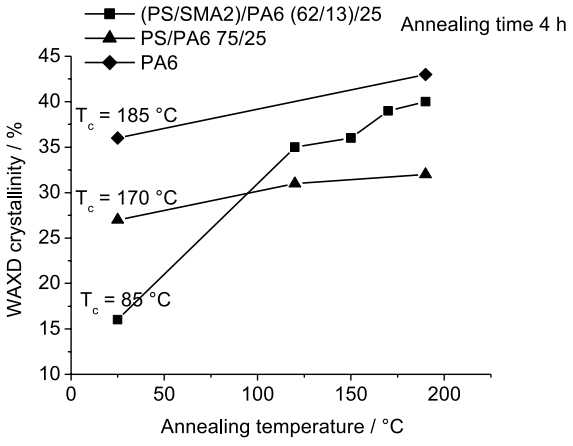

Fig. 14. PA6 WAXD profiles at RT of a (PS/SMA2)/PA6 (62/13)/25 blend after different annealing temperatures.

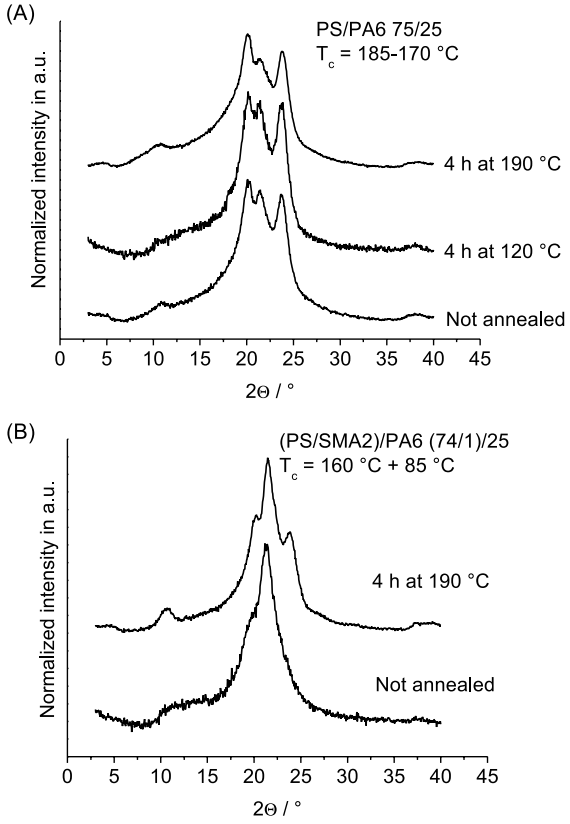

Fig. 15. PA6 WAXD profiles at RT after different annealing temperatures of a PS/PA6 75/25 blend (A) and a (PS/SMA2)/PA6 (74/1)/25 blend (B).

around 160 °C and around 85–90 °C (see Fig. 6). The PS/PA6 75/25 WAXD profile (Fig. 15(A)) is not significantly changed upon annealing. After annealing at 190 °C, still γ-reflections can be observed around 11 and 21° 2θ, although with a somewhat lower intensity relative to the α-reflections than before annealing. The γ-crystals formed between 170 and 130 °C are thus clearly stable and almost no transition to the α-phase takes place. This observation was actually already confirmed by DSC showing a real γ-melting peak around 210 °C, see Fig.10. Similar stability to the γ→α-transition was obtained for the monoclinic γ-phase obtained via the KI/I_2 treatment of α-crystals [19]. The (PS/SMA2)/PA6 (74/1/25) blend, given in Fig. 15(B), represents a mixture of stable and unstable phases. Before annealing, almost full γ-type reflections are found. On annealing, α-reflections appear. The intensity of the γ-reflections in this blend, however, does not seem to be decreased, as can be seen from the peak around 2θ 11 °. The increase of the α-reflections after annealing can thus be explained via transformation during heating of unstable β/γ-like crystals formed at around 85 °C, whereas the peak at 21° 2θ after annealing can be related to the stable γ-crystals formed at 160 °C. This seems to be confirmed by the ratio of α and γ-reflections after annealing (44/56), which is roughly comparable to the ratio of the DSC crystallization peaks at 85 and 160 °C (35/65), respectively.

The annealing behavior of quenched PA6 is given in Fig. 16. Earlier results obtained by Penel-Pierron et al. [30] for quenched PA6 films indicated that a quenched PA6 film was found to crystallize in the β form. This was concluded from the complete β→α-transition for annealing at 190 °C. A 1 mm thick PA6 sample, which was quenched in liquid N_2, was used in the experiments presented here. It is clearly observed in Fig. 16 that for this sample no complete reorganization to the α phase takes place after annealing at different temperatures, seemingly contrary to the results of Penel-Pierron et al. [30]. This result can be explained by comparing the behavior of a thick (1 mm) quenched PA6 sample with that of a very thin quenched sample using DSC annealing experiments presented in Fig. 17. Two different specimens were prepared as such: a thin transparent one and a thicker opaque one and were annealed in the DSC. As can be seen from Fig. 17(A) the thin, transparent piece gives a single melting peak around 221 °C, preceded by cold crystallization around 70 °C. This melting behavior is identical to the melting of homogeneously crystallized sample; only one extra melting peak is found related to the annealing temperature. The single melting peak obtained after homogeneous nucleation thus strongly resembles the melting behavior of thin quenched PA6. The melting of the thick, opaque PA6 sample, however, results in a double melting peak, and the cold crystallization peak around 70 °C is missing. The first melting peak (no.2) does not disappear upon annealing, resulting in a total of four different melting peaks of the opaque sample after annealing. The melting behavior resembles the melting of the PS/PA6 75/25 blend, with stable γ-crystals formed around 170 °C and melting around 210 °C (note that the DSC annealing once more confirms the presence of a stable γ-form, now melting around 215 °C). This discussion stresses the importance of the quenching step on the resulting crystals formed. The 1 mm thick sample used to measure the WAXD annealing curves presented in Fig. 16 was probably too thick to give a perfect PA6 quenching, so no completely transparent sample as in the case of the thin films in the paper of Penel-Pierron et al. [30] was obtained. As a result of this less

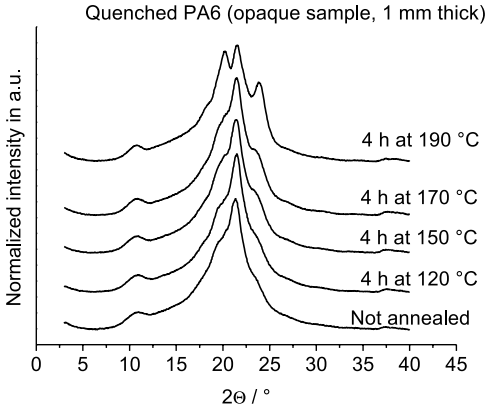

Fig. 16. WAXD profiles at RT of quenched PA6 after different annealing temperatures.

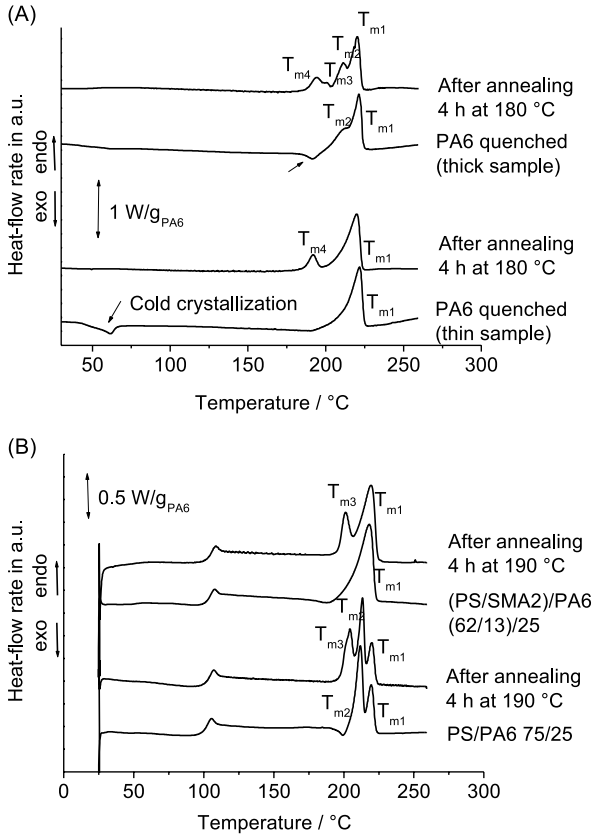

Fig. 17. DSC melting curves before and after annealing of two quenched PA6 samples (A) and a PS/PA6 75/25 blend and a (PS/SMA2)/PA6 (62/13)/25 blend (B).

efficient quenching, it is highly likely that a part of the crystals is crystallized at a higher crystallization temperature. In this way stable γ-crystals could be formed upon quenching. The effect of rapid quenching on the semi-crystalline structures and crystallization kinetics of various polymers was studied in detail by Brucato et al. [49]. The mixture of different crystals formed, therefore can be attributed to the range of actual crystallization temperatures during rapid cooling of PA6. This study further indicates that the hexagonal, mesomorphic β-phase can be obtained by slow cooling of confined, dispersed droplets, and does not necessary have to result from a freezing-in-process as is sometimes anticipated [50,51].

4. Conclusions

In this paper, it was clearly shown that confined crystallization phenomena in immiscible polymer blends with dispersed micro and nanometer sized PA6 droplets form a very effective way to study the stability and crystalline structure of PA6 at different supercoolings. Via a detailed WAXD study, in combination with DSC at different scanning rates, and annealing experiments, it has been shown that a change occurs in PA6 crystal structure from an α to a stable

γ-phase for micrometer sized PA6 droplets (1–10 μm), crystallizing at temperatures between 175 and 130 °C. The formation of the stable γ-phase, with a melting point somewhat below that of the α-phase, was shown to be connected with the lower crystallization temperature and not with the confining volume of the PA6 droplets.

For small, sub-micrometer sized PA6 droplets (100–500 nm), obtained after reactive compatibilization of the blend, a less stable crystal structure is formed around 85 °C, with a WAXD pattern similar to the β-structure proposed for quenched, cold crystallized PA6. The formation of these less ordered PA6 crystals can be related to the homogeneous crystallization mechanism at low temperatures, resulting in a low final PA6 crystallinity. Via a combination of WAXD and DSC annealing experiments, it was shown that upon heating above 50 °C (T_g of PA6), the poorly ordered β-crystals probably first perfection themselves, followed by a complete transition into the α-phase around 170 °C. These crystals finally melt at the melting temperature of α-crystals. Via DSC analysis of a blend sample with several PA6 crystallization peaks, obtained at different degrees of supercooling, we were able to show that the transition between the stable and unstable crystal form approximately takes place around 130 °C.

Acknowledgements

The authors are indebted to the Research Fund of the KULeuven (GOA 98/06), and to the Fund for Scientific Research-Flanders, Belgium for the financial support given to the MSC-laboratory. BG is a postdoctoral fellow of the Fund for Scientific Research-Flanders.

References

[1] Cormia RL, Price FP, Turnbull D. J Chem Phys 1962;37(6):1333.
[2] Koutsky JA, Walton AG, Baer E. J Appl Phys 1967;38(4):1832.
[3] Lotz B, Kovacs AJ. ACS Polym Prepr Div Polym Chem 1969;10(2):820.
[4] Barham PJ, Jarvis DA, Keller A. J Polym Sci Phys Ed 1982;20:1733.
[5] Frensch H, Harnischfeger P, Jungnickel BJ. In: Utracki LA, Weiss RA, editors. Multiphase polymers: blends and ionomers. ACS Symposium series, 395, 1989. p. 101.
[6] Santana OO, Müller AJ. Polym Bull 1994;32(4):471.
[7] Everaert V, Groeninckx G, Aerts L. Polymer 2000;41:1409.
[8] Groeninckx G, Vanneste M, Everaert V. In: Utracki LA, editor. Crystallization, morphological structure and melting of polymer blends. Polymer blends handbook, vol. 8. Dordrecht: Kluwer Academic Publishers; 2002. p. 203–394 [Chapter 3].
[9] Montenegro R, Antonietti M, Mastai Y, Landfester K. J Phys Chem B 2003;107:5088.
[10] Massa MW, Carvalho JL, Dalnoki-Veress K. Eur J Phys E 2003;12(1):111.
[11] Tol RT, Mathot VBF, Groeninckx G. Confined crystallization phenomena in immiscible polymer blends with dispersed micro- and nanometer sized PA6 droplets, part 1: uncompatibilized PS/PA6, (PPE/PS)/PA6 and PPE/PA6 blends. Polymer 2005;46(2):369.
[12] Tol RT, Mathot VBF, Groeninckx G. Confined crystallization phenomena in immiscible polymer blends with dispersed micro- and nanometer sized PA6 droplets, part 2: reactively compatibilized PS/PA6 and (PPE/PS)/PA6. Polymer 2005;46(2):383.
[13] Tol RT, Mathot VBF, Groeninckx G. Confined crystallization phenomena in immiscible polymer blends with dispersed micro- and nanometer sized PA6 droplets, part 3: crystallization kinetics and crystallinity of micro- and nanometer sized PA6 droplets crystallizing at high supercoolings. Polymer 2005 in press.
[14] Illers K-H. Makromol Chem 1978;179:497.
[15] Holmes DR, Bunn CW, Smith DJ. J Polym Sci 1955;17:159.
[16] Wunderlich B. Macromolecular physics. Crystal melting. vol. 3. New York: Academic Press; 1980. pp 70–71.
[17] Tsuruta M, Veda S, Kiruma T. Chem High Polym 1958;15:619.
[18] Arimoto H, Ishibashi M, Hirai M, Chatani Y. J Polym Sci 1965;A3:317.
[19] Illers K-H, Haberkorn H, Simák P. Makromol Chem 1972;158:285.
[20] Kinoshita Y. Makromol Chem 1959;33:1.
[21] Weigel P, Hirte R, Ruscher C. Faseforsch Textiltech 1974;25(198):283.
[22] Murthy NS, Aharoni SM, Szollosi AB. J Polym Sci: Polym Phys Ed 1985;23:2549.
[23] Ziabicki A. Kolliod-Z 1959;167(2):132.
[24] Roldan LG, Kaufmann HS. J Polym Sci Polym Lett Ed 1963;B2:603.
[25] Auriemma F, Petraccone V, Parravicini L, Corradini P. Macromolecules 1997;30:7554.
[26] Stepaniak RF, Garton A, Carlsson DJ, Wiles DM. J Polym Sci: Polym Phys Ed 1979;17:987.
[27] Gianchandani J, Spruiell JE, Clark ES. J Appl Polym Sci 1982;27:3527.
[28] Parker JP, Lindenmeyer PH. J Appl Polym Sci 1977;21:821.
[29] Murthy NS. Polym Commun 1991;32(10):301.
[30] Penel-Pierron L, Depecker C, Séquéla R, Lefebvre J-M. J Polym Sci, Part B: Polym Phys 2001;39:484.
[31] Murthy NS, Bray RG, Correale ST, Moore RAF. Polymer 1995;36(20):3863.
[32] Rotter G, Ishida H. J Polym Sci, Polym Phys 1992;30:489.
[33] Kyotani M, Mitsuhashi S. J Polym Sci: Part A-2 1972;10:1497.
[34] Kyotani MJ. Macromol Sci Phys 1975;B11(4):509.
[35] Illers K-H, Haberkorn H. Makromol Chem 1971;142:31.
[36] Fichera A, Malta V, Marega C, Zannetti R. Makromol Chem 1988;189:1561.
[37] Psarski M, Pracella M, Galeski A. Polymer 2000;41:4923.
[38] Venkatesch GM, Fornes RE, Gilbert RD. J Appl Polym Sci 1983;28:2247.
[39] Miyasaka K, Ishikawa K. J Polym Sci A2 1968;6:1317.
[40] Hiramatsu N, Hirakawa S. Polym J 1982;14:165.
[41] Reichle A, Prietzschk A. Angew Chem 1962;74:562.
[42] Everaert V, Groeninckx G, Pionteck J, Favis BD, Aerts L, Moldenaers P, et al. Polymer 2000;41:1011.
[43] Tol RT, Groeninckx G, Vinckier I, Moldenaers P, Mewis J. Polymer 2004;45(8):2587.
[44] ATHAS data bank, http://web.utk.edu/~athas/databank. For a description see: Wunderlich B. Pure Appl Chem 1995;67:1019.
[45] Gurato G, Fichera A, Grandi FZ, Zannetti R, Canal P. Makromol Chem 1974;175:953.
[46] Khanna YP, Kumar R, Reimschuessel AC. Polym Eng Sci 1988;28(24):1607.
[47] Moon HS, Ryoo BK, Park JK. J Appl Polym Sci, Part B: Polym Phys 1994;32:1427.
[48] Khanna YP. Macromolecules 1992;25:3298.
[49] Brucato V, Piccarolo S, La Carrubba V. Chem Eng Sci 2002;57:4129.
[50] Vasanthan N, Murthy NS, Bray RG. Macromolecules 1998;31:8433.
[51] Murthy NS, Curran SA, Aharoni SM, Minor H. Macromolecules 1991;24:3215.